Chapter 4

Microlensing maps for the Milky Way galaxy

This Chapter compares different models of the Milky Way galaxy and investigates their ability to reproduce the recent results from the microlensing surveys. The maps of microlensing optical depth and microlensing event timescale are constructed. The models are introduced in §4.2 which also presents the results of the optical depth calculation. The dynamical model and event timescale distribution are discussed in §4.3.

4.1 Introduction

Microlensing surveys of the Galaxy are important because they delineate the mass distribution directly. The total number of events identified by the OGLE and MACHO collaborations towards the Galactic Bulge now exceeds a thousand (e.g., Wozniak et al. 2001; Alcock et al. 2000). The identification of events towards spiral arms has been reported by the EROS and OGLE collaborations (Mao 1999; Derue et al. 2001). Maps of optical depth as a function of Galactic latitude and longitude were first drawn by

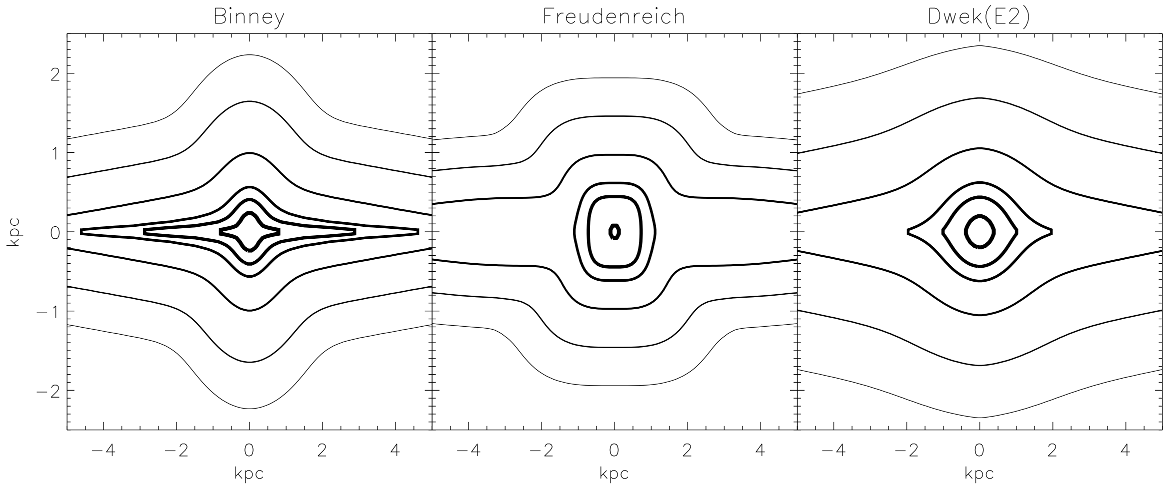

Figure 4.1: Models of the inner Galaxy of Binney et al., Freudenreich and Dwek et al. when viewed along the major axis of the bar. The contour levels are $(10^{-3}, 10^{-2}, 10^{-1}, .5, 1, 2.5) M_\odot\ \mathrm{pc}^{-3}$ and heavier lines correspond to higher density.

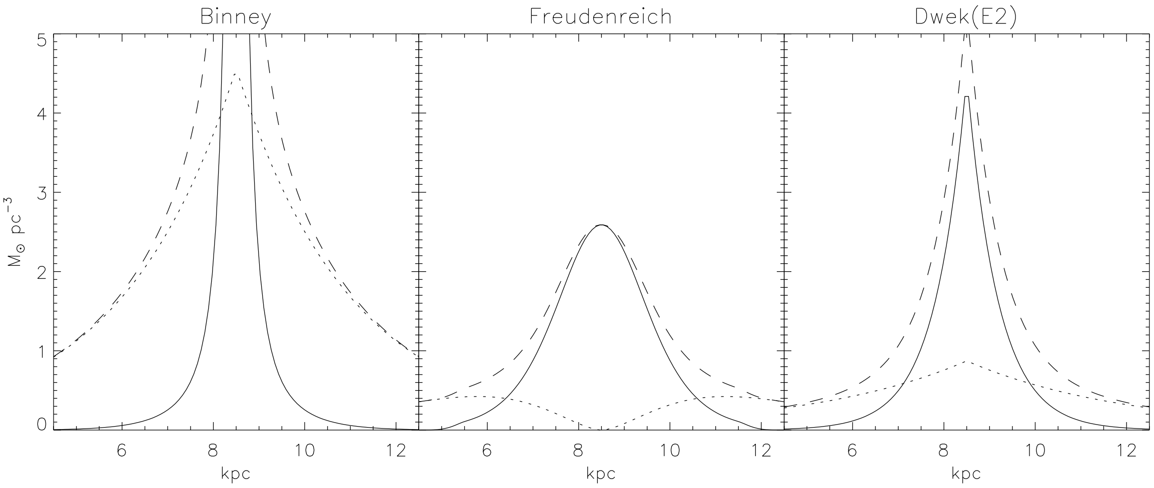

Figure 4.2: Panels show the density contributions of the bar (full line), disk (dotted line) and total (dashed line) along the line of sight to the Galactic Center

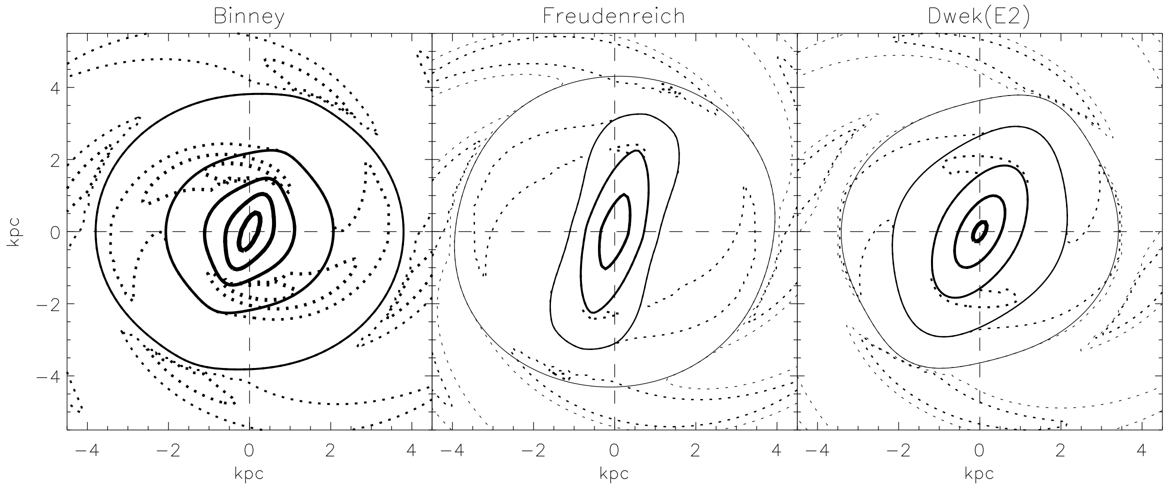

Figure 4.3: Models of the inner Galaxy of Binney et al., Freudenreich and Dwek et al. when viewed from the Galactic Pole. Solid (dotted) lines exclude (include) spirality and Sun-center direction is marked with vertical dashed line (Sun is located at $y = -8.5$ kpc). The contour levels are $(0.33, 0.5, 1, 2, 3, 4, 7) M_\odot$ pc^{-3} and heavier lines correspond to higher density

Evans (1994). Subsequently, a number of authors emphasised the importance of exploiting information on the spatial variation of the optical depth (e.g., Han & Gould 1995; Zhao, Spergel & Rich 1996; Gyuk 1999).

Microlensing searches are being done, or will be done in the near future, in almost any longitude direction. The first of the next generation experiments is the OGLE III venture (see "http://sirius.astrouw.edu.pl/˜ogle/") which uses an 8k×8K MOSAIC camera with a field of view equal to $35' \times 35'$. The future holds still greater promise with the advent of the new class of survey telescopes like the VST ("http://www.eso.org/projects/vst/") and VISTA ("http://www.vista.ac.uk"). VISTA has a field of view of 2.25 square degrees in the optical, while the VST has a smaller, but still substantial, field of view of 1 square degree. So, there is a need for large-scale maps of both the microlensing optical depth and the mean timescale for the Galaxy. These maps can be used to pick target fields, to plan search methodologies for future experiments and to assess what can be learnt about the structure of the Milky Way from the distribution of microlensing events.

Model	bar < 2.5 kpc	disk < 2.5 kpc	bar+disk < 2.5 kpc	disk < 8.5 kpc	inner spiral 3.5 kpc	outer spiral 8.5 kpc
Binney et al	0.5	1.0	1.5	3.2	0.3	0.9
Freudenreich	1.1	0.4	1.5	3.1	0.2	1.2
Dwek et al	0.8	0.7	1.5	3.0	0.2	1.0

Table 4.1: This table shows the mass (in units of $10^{10} M_{\odot}$) in different components of the Galaxy in the three models. The fifth column is the additional mass within 3.5 kpc caused by the inner spiral alone. The sixth column is the additional mass within 8.5 kpc caused by the outer spiral alone.

4.2 Optical depth maps

We study three models of the inner Galaxy. The starting point of all three models is the same, namely the infrared surface brightness maps seen by the DIRBE instrument on the COBE satellite. The first is the model of Binney, Gerhard & Spergel (1997), which is partially revised in Bissantz et al. (1997). Here, the observed luminosity at ~ 240 microns, which is dominated by thermal emission from dust, is used to deduce the three-dimensional spatial distribution of the dust. This gives a short, flattened, cuspy bar with axis ratio $1 : 0.3 : 0.3$ and with a viewing angle $\phi_0 = 20°$. The second is the model of Freudenreich (1998). Here, a mask of areas believed to be contaminated with dust is constructed from maps of color variations. The mask is used to excise portions of the DIRBE data and the remainder of the data is fitted. Note that the mask removes almost all of the data within $|b| \lesssim 5°$ for longitudes within $90°$ of the Galactic Center (see Figure 1 of Freudenreich's paper). This gives an extended, diffuse, swollen bar with axis ratio $1 : 0.37 : 0.27$ and with a viewing angle $\phi_0 = 14°$. The disk has a central hole with a radius of ~ 3 kpc. The third is the E2 model of Dwek et al. (1995), as partially revised by Stanek et al. (1997). The density contours are stratified on concentric ellipses with axis ratio $1 : 0.42 : 0.28$ with a viewing angle $\phi_0 = 24°$. In correcting for dust, Dwek et al. assumed a uniform foreground screen. The bar is less massive and less elongated than Freudenreich's and the disk does not have a central hole. To ensure a fair comparison, all

source	bar	bar	bar
lens	bar	disk	bar+disk
Binney et al	0.28	0.60 (0.88)	0.88 (1.16)
Freudenreich	0.93	0.92 (1.38)	1.85 (2.31)
Dwek et al	0.48	0.73 (1.03)	1.21 (1.51)

Table 4.2: Optical depth to the red clump giants towards $\ell = 3^\circ.9$, $b = -3^\circ.8$ in units of 10^{-6}. Recall that Popowski et al.'s (2000) value for the optical depth to the red clump is $2.0 \pm 0.4 \times 10^{-6}$, which should be compared to the numbers in the last column. The figures in parentheses include the effects of spiral structure (the extra enhancement in the optical depth comes mainly from the extra mass in the spiral models).

source	bar	bar	disk	disk	bar+disk
lens	bar	disk	bar	disk	bar+disk
Binney et al	0.13	0.31 (0.37)	0.13 (0.13)	0.26 (0.37)	0.83 (0.98)
Freudenreich	0.66	0.70 (0.92)	0.13 (0.15)	0.13 (0.22)	1.62 (1.87)
Dwek et al	0.25	0.40 (0.49)	0.25 (0.27)	0.30 (0.43)	1.21 (1.42)

Table 4.3: Optical depth to the main sequence stars towards $\ell = 2^\circ.68$, $b = -3^\circ.35$ in units of 10^{-6}. The total microlensing optical depth reported by Alcock et al. (2000) is $2.43 \pm 0.39 \times 10^{-6}$, which can be compared to the numbers in the last column. The figures in parentheses include the effects of spiral structure.

three models are normalized to have the same total mass of $1.5 \times 10^{10} M_\odot$ within 2.5 kpc. Optical depths scale in rough proportion with total mass, and so our results can be easily converted to other preferred values. The three models are illustrated in Figures 4.1, 4.2 and 4.3. Figures 4.1 and 4.3 show cuts through the principal planes of the bar, while Figure 4.2 shows density contributions of different Galactic components along the line of sight to the Galactic Center. Table 4.1 shows the masses of the components in the three models. Freudenreich's bar is the most massive, Binney et al.'s the least massive.

EROS and OGLE are looking towards spiral arms. Accordingly, we include the effects of spiral arms in our calculations. We assume that the inner spiral pattern is two-armed and given by multiplying the density by eqn (2) of Binney et al. (1997), namely

$$1 + \epsilon \cos^6(\phi - 0.95(r - r_{\min}) - \phi_0), \qquad \epsilon = \tanh(r - r_{\min}). \tag{4.1}$$

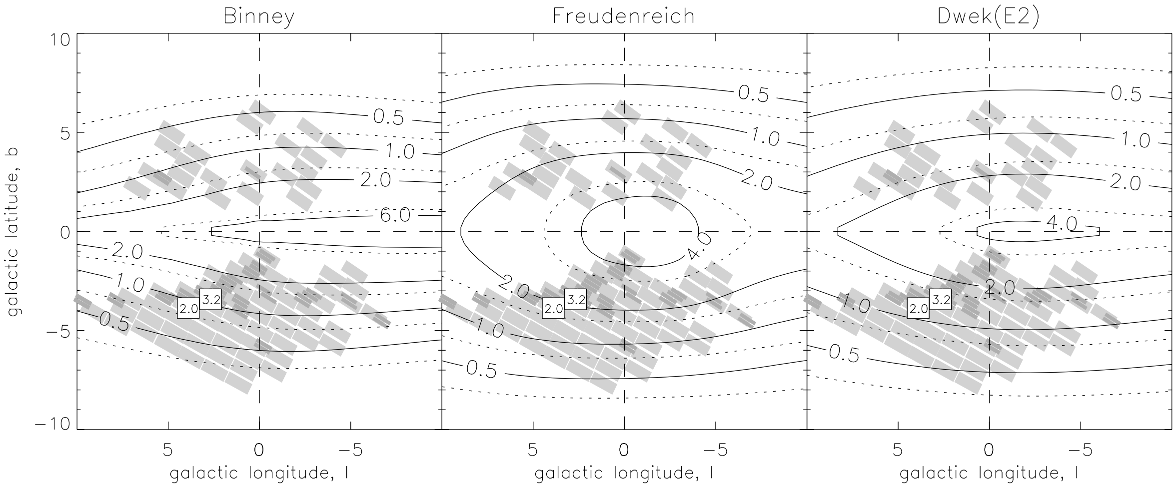

Figure 4.4: Contours of microlensing optical depth to the red clump giants (in units of 10^{-6}) in the three bar models, excluding (full lines) and including (dotted lines) spirality. The optical depths reported by Alcock et al. (2000) and Popowski et al. (2000) are shown in boxes. Light (dark) gray boxes correspond to EROS (OGLE II) fields.

Here, $r_{\rm min}$ is proportional to the length of the bar and is 1.5 kpc for Binney et al.'s bar, 2.25 kpc for Freudenreich's and 1.7 kpc for Dwek et al.'s. This density factor is applied between $r_{\rm min}$ and $r_{\rm max} = 3.5$ kpc. The outer spiral pattern is four-armed and given by $1+2\epsilon\cos^6(2\phi - 1.1(r - r_{\rm min}) - 15^\circ)$ between $r_{\rm min} = 4.1$ kpc and $r_{\rm max} = 8.5$ kpc. The phase and the wavenumber of the inner and outer spirals are chosen to match the longitudes of the principal spiral arms given by Englmaier (2000). The arm/interarm contrast is 2 for the inner and 3 for the outer spiral (cf. Rix & Rieke 1993). This is reasonable for a young population, but an overestimate for old low mass stars that may make up the bulk of the lensing population. Our results on the effects of spirality are upper limits. Figure 4.3 illustrates the effects of spirality (dotted lines) on the density distribution for all three models. Microlensing maps show contours of the source-averaged microlensing optical depth $\langle\tau\rangle$ computed via (Kiraga & Paczyński 1994)

$$\langle\tau\rangle = \frac{\int_0^\infty \rho(D_{\rm s})\tau(D_{\rm s})D_{\rm s}^{2+2\beta}dD_{\rm s}}{\int_0^\infty \rho(D_{\rm s})D_{\rm s}^{2+2\beta}dD_{\rm s}}, \tag{4.2}$$

where $D_{\rm s}$ is the source distance and ρ is the density of deflectors. For red clump stars,

Direction	θ Mus	γ Nor	γ Sct	β Sct
EROS	< 0.68	$0.27^{+0.30}_{-0.17}$	$1.64^{+0.92}_{-0.74}$	< 1.03
Binney et al	0.34 (0.44)	0.56 (0.93)	0.80 (1.11)	0.65 (0.85)
Freudenreich	0.44 (0.50)	0.86 (1.45)	1.13 (1.49)	1.00 (1.30)
Dwek et al	0.39 (0.52)	0.63 (1.00)	0.94 (1.28)	0.75 (1.00)

Table 4.4: Optical depth towards spiral arms in units of 10^{-6}. The figures in parentheses include the effects of spiral structure. The numbers should be compared with the experimental data provided by the EROS collaboration (Derue et al. 2001) in the second line.

$\beta \approx 0$; for main sequence stars, $\beta \approx -1$. Red clumps stars are bright and distinctive residents of the bar (e.g., Paczyński & Stanek 1998). In other words the estimates of the optical depth to these standard candles are free from systematic uncertainties such as blending and contamination by disk stars. Figure 4.4 shows contours of optical depth to the red clump in the three models. The dotted contours show the effect of including the spiral structure. The amplification caused by spirality varies according to the line of sight but it is typically $\sim 20\%$. Of the three, Binney et al.'s gives the least symmetric microlensing map, especially close to the Galactic plane where the gradients are very steep. Freudenreich's is the most symmetric, as it possesses the smallest viewing angle. The boxes mark the two locations where the optical depth of bar stars has been measured. The first is $\ell = 3.9°, b = -3.8°$ where Popowski et al. (2000) report $2.0 \pm 0.4 \times 10^{-6}$ for the optical depth to the red clump stars. The second is $\ell = 2.68°, b = -3.35°$ where Alcock et al. (2000) report $3.2 \pm 0.5 \times 10^{-6}$ for the optical depth to bar stars. The value of the optical depth at $\ell = 3.9°, b = -3.8°$ contributed by each component in the three models is recorded in Table 4.2. Freudenreich's model is in good agreement with the two measurements of optical depth to the bar sources. The value of the optical depth to the main sequence stars at the location $\ell = 2°.68$, $b = -3°.35$ is given in Table 4.3. This can be compared to the total microlensing optical depth of $2.43 \pm 0.39 \times 10^{-6}$ reported by Alcock et al. (2000). Even though all three models have the same total mass within 2.5 kpc, Freudenreich's model has the higher optical depth because the bar is more extended.

Notice that the shape of the contours in Figure 4.4 becomes very similar for all three models once $|b| > 4°$. This makes it challenging to characterize the bar morphology on the basis of data from the observed fields. One qualm is that Freudenreich excised most of the DIRBE data within $|b| \lesssim 5°$ of the Galactic plane. In this region, his model is entirely extrapolated from the light distribution at higher latitudes and so may be unreliable. Binney et al.'s model reproduces the strong concentration in the light near the Galactic plane. It lies within $\approx 2\sigma$ of Popowski et al.'s measurement when spiral structure is included. Dwek et al.'s model with spiral structure is just outside 1σ. Can we modify Binney et al.'s model to reproduce the microlensing optical depth data? To get agreement with the data, the bar needs to be made both longer and fatter. For example, changing the axis ratio to $1 : 0.6 : 0.4$ (as originally envisaged in Binney et al. 1997) and increasing the total mass within 2.5 kpc by 50% gives a model in reasonably good agreement (namely $\tau = 1.5 \times 10^{-6}$ at $\ell = 3.9°, b = -3.8°$ excluding spiral structure; this rises to 1.8×10^{-6} when spiral structure is included). Figure 4.5 shows the contours of optical depth to all sources in the inner Galaxy using Freudenreich's bar. The Galactic disk has a sech-squared vertical profile with scaleheight 167 pc and an exponential horizontal profile with scalelength 2.5 kpc. The insets show the details of three areas towards the Scutum, Norma and Musca spiral arms that are being monitored by the EROS group. We see that there is a factor of ~ 6 variation in the optical depth across the EROS fields towards all three spiral arms. Freudenreich's bar is so distended that it causes a thickening of the optical depth contours even at longitudes well away from the center. We can exploit the maps to estimate the number of ongoing microlensing events of stars brighter than 20th magnitude in the Milky Way. At any instant, there are ~ 500 microlensing events, where we have allowed for extinction in the same manner as in Chapter 5 and Chapter 6. Table 4.4 compares the predictions of the three models with the data provided by EROS. Notice that all three models are in a reasonable agreement with the EROS measurements (although Freudenreich's model

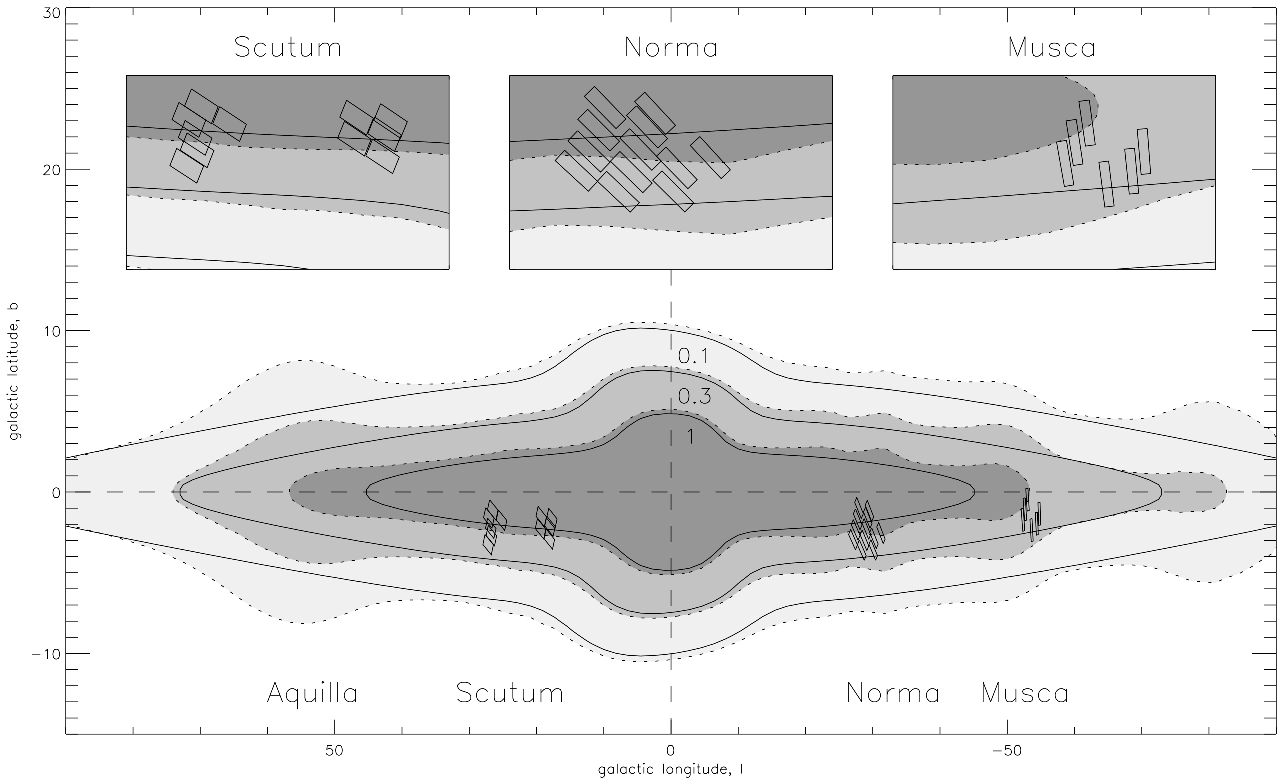

Figure 4.5: Contours of microlensing optical depth to all sources (in units of 10^{-6}) in Freudenreich's model, excluding (full lines) and including (dotted lines) spiral structure. The insets show the details of EROS fields towards the Scutum, Norma and Musca spiral arms.

performs somewhat better) except for the field γ Norma. This field – located at $\sim 30°$ from the Galactic centre – is believed to provide a measure of disk lensing in the Galaxy. All three models give a value of optical depth about $1-2\sigma$ above the data which indicates that the bar contribution is probably over-estimated.

4.3 Timescale map

It is also interesting to build maps of the mean Einstein crossing timescale. We assume that the mass function of the bar (or disk) is a power-law between $0.01M_\odot$ and $0.5M_\odot$ with index -1.33 (or -0.54) as suggested by Zoccali et al. (2001). Let (x, y, z) define coordinates along the major, intermediate and minor axis of the bar. We calculate the average velocity dispersions required to reproduce the shape of Freudenreich's bar guided by the tensor virial theorem (e.g., Han & Gould 1995, Blum 1996), however the pattern speed of the bar is not taken into account. The velocity distribution is Gaussian with dispersions $\sigma_x = 100\,\mathrm{km\,s^{-1}}$, $\sigma_y = 80\,\mathrm{km\,s^{-1}}$, $\sigma_z = 68\,\mathrm{km\,s^{-1}}$. For the disk lenses, the random component has $\sigma_R = 34\,\mathrm{km\,s^{-1}}$, $\sigma_\phi = 21\,\mathrm{km\,s^{-1}}$, $\sigma_z = 18\,\mathrm{km\,s^{-1}}$ about a mean velocity $\langle v_\phi \rangle$ of $214\,\mathrm{km\,s^{-1}}$ (see Chapter6). The velocity of the Sun has the following components: $v_{\odot R} = -10\,\mathrm{km\,s^{-1}}$ $v_{\odot\phi} = 219.25\,\mathrm{km\,s^{-1}}$ and $v_{\odot z} = 7.17\,\mathrm{km\,s^{-1}}$ (Dehnen & Binney 1998). Although small velocity perturbations will be associated with the spiral arms, these are neglected in our calculations. Figure 4.6 shows contours of the source-averaged timescale for events with sources and lenses in either the disk or Freudenreich's bar, including (dotted lines) and excluding (full lines) the spiral structure. The timescale is shortest towards the Galactic Center and becomes longer at increasing Galactic longitudes. This is easy to understand because the motion of the lens is directed more and more along the line of sight at larger longitudes and so the transverse velocity is typically smaller. Notice that spiral structure has a dramatic effect on the timescale. For example, at Baade's Window, the timescale is increased by a factor of $\sim 50\%$ on

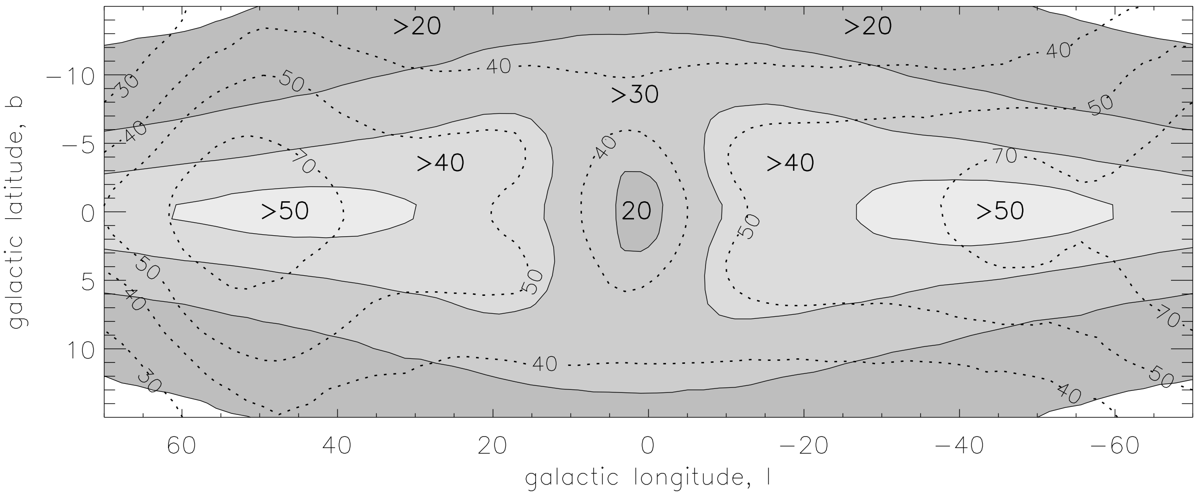

Figure 4.6: Contours of source-averaged timescale (in days) for microlensing events with sources and lenses lying in either the disk or Freudenreich's bar. The timescale is the time taken to cross the Einstein radius. The full lines exclude the contribution of spiral structure, the dotted lines include the contribution. The contour levels are at $20, 30, 40, 50, 60$ and 70 days .

incorporating the effects of spirality. At the locations around $|l| \sim 60^\circ$ the timescale is doubled by the effect of spirality.

4.4 Conclusions

We have drawn large scale maps of the optical depth and timescale distribution for microlensing in the Galaxy. Freudenreich's bar does give a reasonable representation of the microlensing data to the Bulge. It recovers the optical depth towards the spiral arms (with the exception of γ Norma). However, Freudenreich's model is hollow. Stars otherwise expected to be in the central parts of the disk can instead be used to augment the bar where they are efficient at microlensing.

As pointed out by Gould (1995), microlensing surveys in the K band would be very valuable to distinguish between models. This is all the more true given the capabilities of the new generation of survey telescopes. VISTA has a field of view of 0.5 square degrees in the K band. Assuming that the seeing is $0.8''$ in Chile and scaling the results of Gould (1995), then we estimate that VISTA will monitor $\sim 1.5 \times 10^6$ stars in a single field of view for crowding-limited K band images towards the Bulge. This means that we are probing the luminosity function down to $K \sim 16$, assuming 3 magnitudes of extinction. Photometry accurate to 3% for a $K \sim 16$ star will take ~ 1 minute on VISTA. Hence, a K band survey of a $5^\circ \times 5^\circ$ field close to the Galactic Center will take ~ 100 minutes every night, allowing 50 minutes for readout, slew and guide star acquisition time. So, a K band microlensing survey of the inner Galaxy is an attractive and feasible proposition with VISTA.

4.5 Bibliography

Alcock C. et al. 2000, ApJ, 541, 734

Binney J., Gerhard O., Spergel D. 1997, MNRAS, 288, 365

Bissantz N., Englmaier P., Binney J., Gerhard O.E. 1997, MNRAS, 289, 651

Blum R. 1995, ApJ, 444, L89

Derue F. et al. 2001, AA, 373, 126

Dwek E. et al. 1995, ApJ, 445, 716

Edvardsson B., Andersen J., Gustafsson B., Lambert D.L., Nissen P.E., Tomkin J. 1993, A&AS, 102, 603

Englmaier P., 2000, Rev Modern Astronomy, 13, 97

Evans N.W., 1994, ApJ, 437, L31

Gould A. 1995, ApJ, 446, L71

Gyuk G. 1999, ApJ, 510, 205

Han C., Gould A. 1995, ApJ, 449, 521

Kiraga M., Paczyński B. 1994, ApJ, 430, L101

Mao S. 1999, AA, 350, L19

Paczyński B., Stanek K.Z. 1998, ApJ, 494, L219

Popowski P. et al. 2000, In Menzies J.W., Sackett P.D. eds, Proc. Microlensing 2000, ASP Conference Series, in press (astro-ph/0005466)

Rix H.W., Rieke M.J. 1993, ApJ, 418, 123

Stanek K.Z., Udalski A., Szymanski M., Kaluzny J., Kubiak M., Mateo M., Krzeminski W. 1997, ApJ, 477, 163

Wozniak P.R., Udalski A., Szymanski M., Kubiak M., Pietrzynski G., Soszynski I., Zebrun K. 2001, Acta Astronomica, 51, 175

Zhao H.S., Rich R.M., Spergel D.N. 1996, MNRAS, 282, 175

Zoccali M., Cassisi S., Frogel J.A., Gould A., Ortolani S., Renzini A., Rich R.M., Stephens A.W. 2000, ApJ, 530, 418